Molecular Cell, Vol. 17, 193–203, January 21, 2005, Copyright ©2005 by Elsevier Inc. DOI 10.1016/j.molcel.2004.11.047

Crystal Structure of the Ligand Binding Suppressor Domain of Type 1 Inositol 1,4,5-Trisphosphate Receptor

Ivan Bosanac,[1] Haruka Yamazaki,[2] Toru Matsu-ura,[3,4] Takayuki Michikawa,[2,3] Katsuhiko Mikoshiba,[2,3,4,5] and Mitsuhiko Ikura[1,*]

[1]Division of Molecular and Structural Biology
Ontario Cancer Institute and
Department of Medical Biophysics
University of Toronto
610 University Avenue
Toronto, Ontario, M5G 2M9
Canada

[2]Calcium Oscillation Project
International Cooperative Research Project
Japan Science and Technology Agency
Tokyo 108-0071
Japan

[3]Division of Molecular Neurobiology
Department of Basic Medical Sciences
Institute of Medical Science
University of Tokyo
Tokyo 108-8639
Japan

[4]Laboratory for Developmental Neurobiology
Brain Science Institute
RIKEN
Saitama 351-0198
Japan

[5]Division of Neural Signal Information NTT-IMSUT
Department of Basic Medical Sciences
Institute of Medical Science
University of Tokyo
Tokyo 108-8639
Japan

Summary

Binding of inositol 1,4,5-trisphosphate (IP_3) to the amino-terminal region of IP_3 receptor promotes Ca^{2+} release from the endoplasmic reticulum. Within the amino terminus, the first 220 residues directly preceding the IP_3 binding core domain play a key role in IP_3 binding suppression and regulatory protein interaction. Here we present a crystal structure of the suppressor domain of the mouse type 1 IP_3 receptor at 1.8 Å. Displaying a shape akin to a hammer, the suppressor region contains a Head subdomain forming the β-trefoil fold and an Arm subdomain possessing a helix-turn-helix structure. The conserved region on the Head subdomain appeared to interact with the IP_3 binding core domain and is in close proximity to the previously proposed binding sites of Homer, RACK1, calmodulin, and CaBP1. The present study sheds light onto the mechanism underlying the receptor's sensitivity to the ligand and its communication with cellular signaling proteins.

*Correspondence: mikura@uhnres.utoronto.ca

Introduction

A central mechanism for calcium (Ca^{2+})-regulated cellular processes involves release of Ca^{2+} from the intracellular endoplasmic reticulum (ER) Ca^{2+}-stores into the cytoplasm. In a variety of cells, this Ca^{2+} signaling process is mediated by the ER membrane-associated Ca^{2+} release channel, inositol 1,4,5-trisphosphate receptor (IP_3R) (Berridge, 1993; Berridge et al., 2003). As a signal transducer between the two ubiquitous second messengers D-*myo*-inositol 1,4,5-trisphosphate (IP_3) and Ca^{2+}, IP_3R plays a crucial role in the control of cellular and physiological processes as diverse as cell division, cell proliferation, apoptosis, fertilization, development, behavior, memory, and learning (Furuichi and Mikoshiba, 1995). In *Xenopus* embryos, IP_3R has been implicated in the modulation of ventral differentiation (Kume et al., 1997), while mice lacking type 1 IP_3R display cerebellar ataxia and epileptic seizures (Matsumoto et al., 1996).

IP_3Rs are highly ubiquitous and have been found in organisms ranging from humans to *C. elegans*. Mammalian IP_3R has three distinct isoforms with identical molecular architecture by which they form homo- or heterotetrameric functional channels (Taylor et al., 1999). Mouse type 1 IP_3R (mIP_3R1), found in high abundance in cerebellar Purkinje cells (Worley et al., 1987), is a polypeptide of 2749 amino acids with five functionally distinct regions (Figure 1A): the N-terminal IP_3 suppressor and IP_3 binding regions, the central modulatory region, and the C-terminal channel and the coupling regions. The ligand binding core construct (residues 224–579) has been shown to possess high affinity for IP_3 (K_d = 2.3 nM) (Yoshikawa et al., 1996). This high affinity is attenuated to a physiological range (K_d = 45 nM) by the presence of the N-terminal suppressor domain (IP_3R_{sup}) (Yoshikawa et al., 1999b).

In addition to its involvement in IP_3 suppression, the first 223 residues of the receptor are known to bind a number of cellular proteins that modulate the receptor. Calmodulin (CaM) is one such protein, whose docking site was mapped to two independent segments within the first 160 residues of the receptor (Sienaert et al., 2002). This interaction was observed in the presence and in the absence of the Ca^{2+} with a role in IP_3-induced Ca^{2+} release (IICR) inhibition (Kasri et al., 2004a). Foskett and coworkers (Yang et al., 2002) reported Ca^{2+}-dependent association of the neuronal Ca^{2+} binding protein 1 (CaBP1) with the first 600 residues of the IP_3R and found it to be responsible for direct activation of the receptor in the absence of the IP_3. In contrast, recent study (Kasri et al., 2004b) reported CaBP1 binding to one of the CaM binding sites to be Ca^{2+} independent and CaBP1 serving as an antagonist rather than an agonist. One of the two IP_3R segments (residues 90–110 and residues 580–600) necessary for binding RACK1 resides within the IP_3R_{sup} (Patterson et al., 2004). Interaction of IP_3R with group 1 metabotropic glutamate receptors (mGluRs) is mediated by Homer proteins which bind to the ^{49}PPKKF^{53} stretch on the mIP_3R1 (Tu et al., 1998).

A number of 3D EM structures of the overall receptor

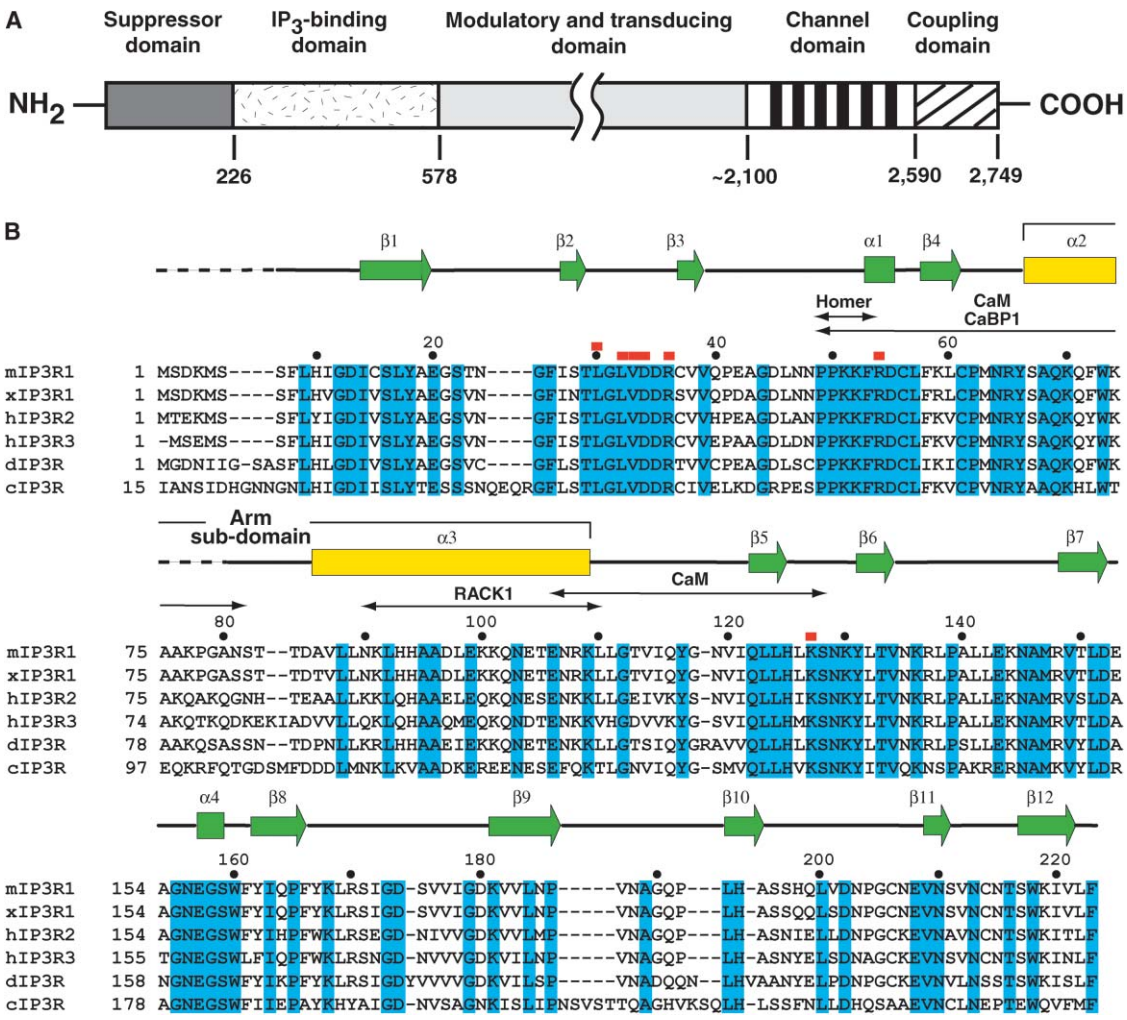

Figure 1. Overall Molecular Architecture of IP_3R and Sequence Alignment of the Suppressor Domain between Members of the IP_3R Family

(A) The five functional domains of mIP_3R1 from left (N terminus) to right (C terminus): suppressor domain, IP_3 binding domain, modulatory and transducing domain, channel domain (putative membrane spanning segments shown as solid bars), and coupling domain.

(B) Sequence alignment of the suppressor domain of mIP_3R1 with other members of the IP_3R family. Conserved residues are highlighted in blue. Secondary structural elements deduced from the crystal structure are depicted as follows: β strands (arrows), α helices (bars), and unidentified portions (dotted lines). Structural segments of the Head subdomain and the Arm subdomain are shown in green and yellow, respectively. Red squares represent those residues predicted to be involved in IP_3 suppression. Proposed binding region for Homer (Tu et al., 1998), CaM (Sienaert et al., 2002), CaBP1 (Kasri et al., 2004b), and RACK1 (Patterson et al., 2004) are indicated by double arrowhead lines. National Center for Biotechnology Information (NCBI) accession numbers for sequences used in the alignment are: mouse1 (mIP_3R1, X15373), *Xenopus* (xIP_3R, D14400), human2 (hIP_3R2, D26350), human3 (hIP_3R3, D26351), *Drosophila* (dIP_3R, D90403), and *C. elegans* (cIP_3R, AJ243181).

have recently been elucidated (da Fonseca et al., 2003; Hamada et al., 2003; Jiang et al., 2002; Sato et al., 2004; Serysheva et al., 2003). They all exhibit 4-fold symmetry reflecting the tetrameric organization of the receptor. Moreover, two distinct domains are identified within these structures, with the larger one encompassing the cytoplasmic portion of the receptor and the smaller one the transmembrane (TM) and luminal region. Positioning of the atomic-resolution structure of the IP_3 binding core (IP_3R_{core}) (Bosanac et al., 2002) was possible within the cytoplasmic domain; however, due to the resolution limit of EM-derived structures, not much detail was obtained for the IP_3R_{sup} region. A study by Hamada et al. demonstrated that Ca^{2+} binding induces a conformational change in the tetrameric receptor from the closed state (square shaped) to the open state (windmill shaped) (Hamada et al., 2003).

The closest relatives of the IP_3Rs are ryanodine receptors (RyR), which also serve as intracellular Ca^{2+} channels (Berridge et al., 2003). The two receptors share the highest sequence homology within the N-terminal and TM regions (Furuichi et al., 1994). Conservation within the TM region may be due to their conductance of Ca^{2+} ions, whereas the homology within the N terminus is unclear since RyR lacks the ability to bind IP_3. Recent bioinformatic analysis of the N-terminal residues of the two receptors proposes a similar structural arrangement for this region (Ponting, 2000). This similarity may suggest a common function not yet identified.

The mechanism by which IP_3R_{sup} inhibits IP_3 binding

Table 1. Data Collection and Refinement Statistics for IP_3R_{sup} Structure

Data Collection

Data Set	Wavelength (Å)	Resolution(Å)	Reflections (Total/Unique)	Completeness (%)	R_{merge}[a] (%)	$\langle I/\langle\sigma(I)\rangle\rangle$[b]
λ_1	0.9795	19.5–1.9	910,987/21,416	99.6 (100)	6.2 (32.7)	67.3 (7.3)
λ_2	0.9796	19.5–1.9	673,838/21,309	99.6 (100)	5.1 (35.9)	57.4 (5.5)
λ_3	0.9641	19.5–1.9	771,369/21,328	99.5 (100)	5.1 (41.2)	53.3 (4.9)
Native	0.9951	50.0–1.8	1,537,463/25,011	100 (100)	4.4 (22.1)	83.8 (10.8)

Refinement Statistics

Data Set	Resolution (Å)	Reflections (Working/Test)	Total Number of Atoms	R_{cryst}[c]/R_{free}[d]	$\langle B\rangle$ Value (Å^2)	Rms Deviations	
						Bond (Å)	Angle (°)
Native	50.0–1.8	23,162/1,187	1,841	20.5/23.8	36.2	0.007	1.5

[a] $R_{merge} = \Sigma_h\Sigma_i|I_{hi} - \langle I_h\rangle|/\Sigma_h\Sigma_i|\langle I_h\rangle| \times 100$, where I is the intensity of i observations for reflection h and I_h is the mean intensity of the reflection.
[b] $\langle I\rangle/\langle\sigma I\rangle$, mean intensity/mean standard deviation.
[c] $R_{cryst} = 100 \times \Sigma||F_{obs}| - |F_{calc}||/\Sigma|F_{obs}|$, where F_{obs} and F_{calc} are the observed and calculated structure factor magnitudes, respectively.
[d] R_{free} as for R_{cryst} except calculated for 4.7% of the reflections not used for model refinement.

to the IP_3R_{core} of the receptor is largely lacking. The role of the IP_3R_{sup} has been thought to modulate IP_3 affinity by masking the IP_3 binding site such that IP_3 cannot freely approach its docking location. In order to gain atomic-level insights into the mechanism underlying IP_3 suppression, we determined the atomic-resolution structure of IP_3R_{sup}. This portion of the receptor is composed of a single domain with the same fold as one of the IP_3R_{core} domains (Bosanac et al., 2002). Site-directed mutagenesis identified seven surface residues on IP_3R_{sup} to be involved in the IP_3-suppression mechanism. Interestingly, docking sites for a number of binding partners reside in close proximity to these residues. The presence of the same domain organization within the N terminus of the RyRs will be discussed.

Results and Discussion

Structure Determination and the Global Fold

A protein fragment encompassing residues 2–223 of mIP_3R1, which corresponds to the suppressor domain of the IP_3R (IP_3R_{sup}), was cloned with an N-terminal T7-tag and C-terminal poly-His tag. The resulting fusion protein was expressed in *E. coli*, purified to homogeneity, and subjected to crystallization experiments. The crystals of both the native protein and the selenomethionine (Se-Met)-incorporated protein were obtained at room temperature. Three-wavelength multiple anomalous dispersion (MAD) data were collected on the Se-Met crystals and were subsequently used for structure determination. The final molecular model (comprising residues 7–75 and 82–223) was refined to 1.8 Å resolution with a free R value of 23.8 and a conventional R value of 20.5 (structural statistics are summarized in Table 1).

IP_3R_{sup} forms a hammer-like structure with approximate dimensions of $63 \times 44 \times 41$ Å^3. The Head subdomain of the hammer consists of 12 β strands and 2 single-turn α helices, together constituting a globular core region (Figures 2A and 2B). The β strands are arranged into six two-stranded hairpins, three of which form a barrel, while the other three form a triangular array that caps the top of the barrel. The 45 Å long Arm subdomain of the hammer, made of a helix-turn-helix structure, protrudes away from the core segment. This helix-turn-helix segment is inserted between β4 and β5 of the core region and a portion of the interhelical turn (residues 76–81) is not visible in the crystal structure presumably due to the intrinsic flexibility of this region.

Visual inspection of the structure, as well as analysis by a DALI algorithm (Holm and Sander, 1993), indicated that IP_3R_{sup} contains the well-known fold of β-trefoil type. This fold was previously identified in the crystal structure of the IP_3R_{core} in the region of residues 224–434 (Bosanac et al., 2002). Therefore, the N-terminal region of IP_3R consists of two β-trefoil domains, the first corresponding to the IP_3R_{sup} and the latter to half of the IP_3R_{core}, and a "armadillo"-like α-helical domain (residues 438–604) (Bosanac et al., 2002). The presence of multiple β-trefoil folds in a protein structure has been found in other members of the β-trefoil protein family including Ricin B-like (Rutenber and Robertus, 1991), Agglutinin (Transue et al., 1997), and Fascin (1DFC in Protein Data Bank). Despite the low protein sequence identity between the first and second β-trefoil domains of IP_3R (14%), the two domains superimpose well with rmsd of 2.0 Å (Figure 2D). One striking difference between the first and second β-trefoil domains is the presence of the helix-turn-helix module between strands β4 and β5 in the first domain and the presence of a long loop between strands β6 and β7 in the second domain, which contains the splice site SI (Bosanac et al., 2002). Among all members of the β-trefoil protein family whose structures have been solved, the long helix-turn-helix segment in the IP_3R_{sup} represents an extremely unusual insertion to its structural scaffold.

Possible Mechanisms for IP_3R_{sup}-Mediated Modulation of IP_3 Binding

IP_3R N-terminal construct (residues 1–604) containing both IP_3R_{sup} and IP_3R_{core} showed a physiologically relevant affinity for IP_3 which is lower than that of the IP_3R_{core} construct (residues 224–579) (Yoshikawa et al., 1996). The mechanism by which IP_3R_{sup} inhibits IP_3 binding to the ligand binding core of the receptor is largely lacking. In light of IP_3R_{sup} and IP_3R_{core} structures, we have attempted to elucidate this key mechanism in order to

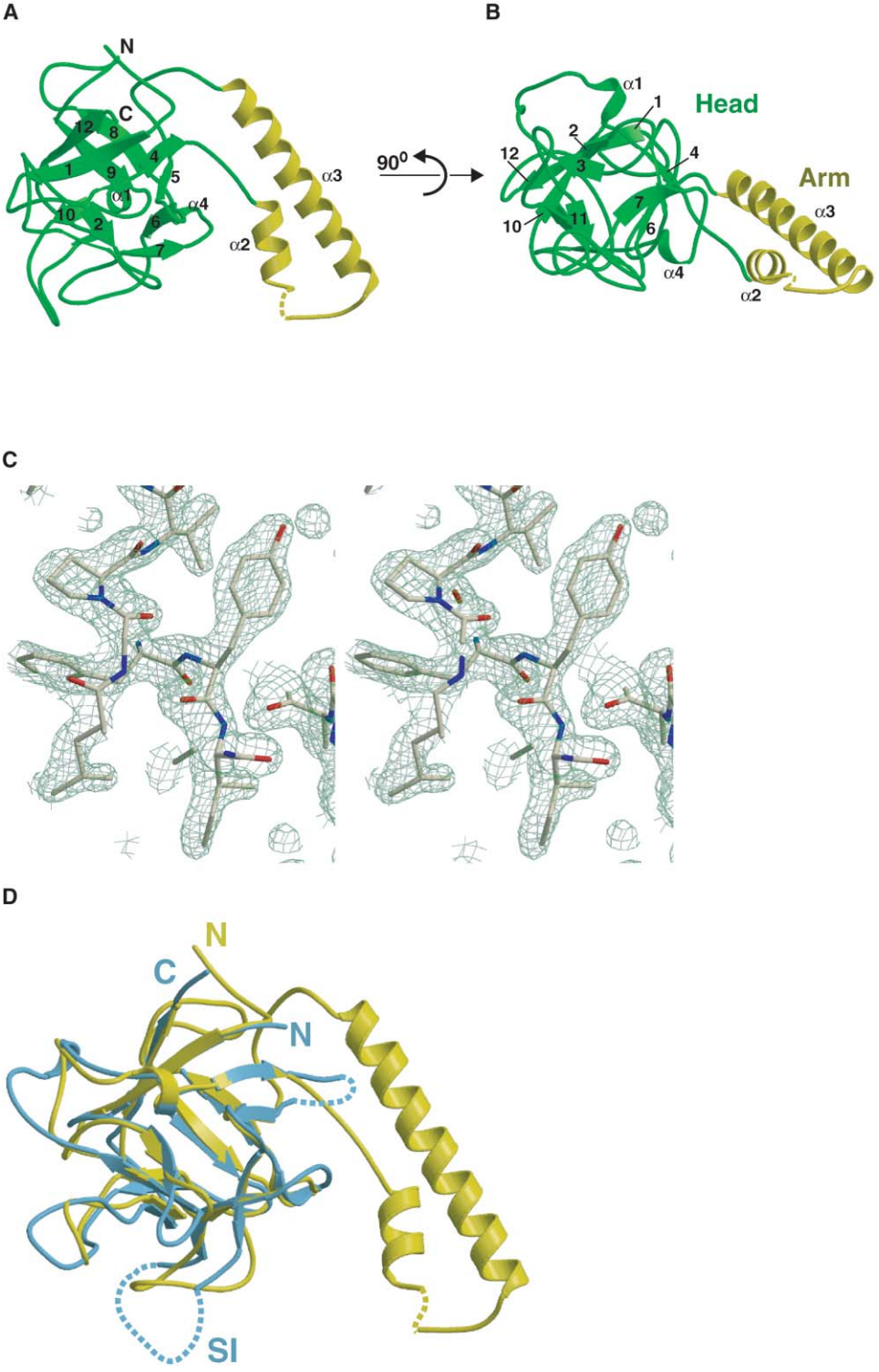

Figure 2. Structure of Mouse IP_3R_{sup}

(A) Ribbon diagram of the IP_3R_{sup} Head subdomain (green) and Arm subdomain (yellow).

(B) View in (A) rotate by 90°.

(C) Section of experimental electron density map contoured at 2.5σ in stereoview.

(D) The IP_3R_{sup} (yellow) is superimposed on the β-domain of the IP_3R_{core} (cyan) (PDB accession number 1N4K, residues 236–436). The splice site SI is shown in β-domain of the IP_3R_{core}. The rmsd of the superposition is 2.0 Å. Panels were generated with MOLSCRIPT (Kraulis, 1991), Raster3D (Merrit and Bacon, 1997), and CONSCRIPT software (Lawrence and Bourke, 2000).

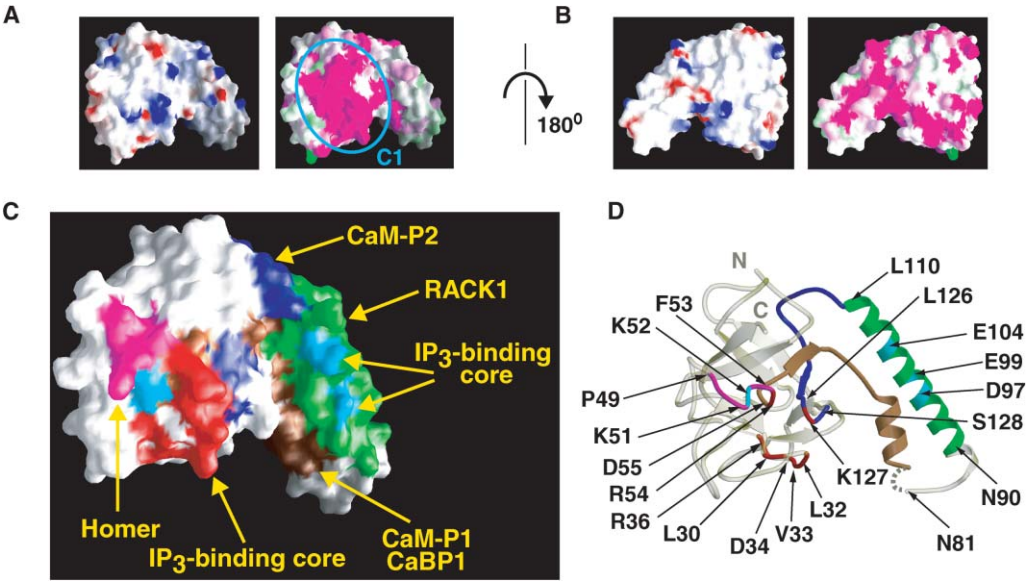

Figure 3. Molecular Surface Characteristics of IP_3R_{sup}

(A) Surface representation of IP_3R_{sup} in the same orientation as Figure 2A. Surface electrostatic potential is shown in the left panel with positive charge depicted in blue and negative charge in red. Surface residue conservation determined from sequence alignment in Figure 1B is plotted with color gradient from magenta (identical residues) to green (least conserved residues) and is presented in the right panel. The highly conserved surface region (C1) is labeled.

(B) View in (A) rotate by 180°.

(C and D) Surface and ribbon diagram representations of key sites on IP_3R_{sup} for binding other proteins. Residues involved in IP_3 suppression are shown in red. Residues in cyan are not involved in IP_3 suppression but may play a part in interaction of IP_3R_{sup} with IP_3R_{core}. Docking sites for Homer (magenta, residues P49–F53) (Tu et al., 1998) and RACK1 (green, residues N90–L110) (Patterson et al., 2004) are shown. Due to the overlap with Homer, RACK1, and the IP_3 binding core, not all residues responsible for binding CaM-P1 and CaBP1 (brown, residues P49–N81) (Kasri et al., 2004b; Sienaert et al., 2002) and CaM-P2 (blue, residues E106–S128) (Sienaert et al., 2002) are colored. Conservation was determined with ConSurf (Armon et al., 2001) and surface representation was generated with GRASP (Nicholls et al., 1991) (A–C). MOLSCRIPT (Kraulis, 1991) and Raster3D (Merrit and Bacon, 1997) were used in (D).

understand the Ca^{2+} release function of the receptor in response to physiological concentrations of IP_3. We first examined whether or not IP_3R_{sup} contains a negatively charged region which may mimic the triphosphate group of IP_3. Manual inspection of IP_3R_{sup} surface identified no extensive charged patches (Figures 3A and 3B). One possible region resides at four acidic residues (D97, E99, E104, and E106), which are all localized to the solvent-exposed surface of the α3 helix of the Arm subdomain. In order to test the involvement of these acidic residues in the IP_3 binding suppression, we initiated extensive mutagenesis and IP_3 binding studies on the construct T604 containing both IP_3R_{sup} and IP_3R_{core}. An excellent IP_3 binding curve was obtained for T604, which yielded a dissociation constant (K_d) of 8.9 nM (Figure 4A). The construct lacking the first 223 residues (Δ(1-223)T604) showed a lower K_d (0.58 nM). A series of lysine or alanine single or double mutations for the acidic residues in the Arm subdomain were made (D97K, E99K, E104K, E106K, D97K/E99A, E104A/E106A), and their IP_3 binding ability was measured (Figure 4B and see Supplemental Table S1 at http://www.molecule.org/cgi/content/full/17/2/193/DC1/). Single mutations of residue D97, E99, or E104 resulted in a significant increase in K_d values (16–18 nM) relative to the value of T604 (8.9 nM), suggesting that they may be involved in the interaction with IP_3R_{core}. On the other hand, only a subtle decrease in the K_d value was observed when the entire Arm subdomain was deleted, suggesting that the Arm subdomain is not critical to the interaction with IP_3R_{core}.

We further performed mutagenesis studies on the most conserved surface region (C1) of the IP_3R_{sup} structure (Figure 3A), and ten residues (Figure 4B) were selected for the substitution with lysine or glutamate. Interestingly, seven of ten mutations resulted in a significant increase in IP_3 binding affinity. The mutation V33K produced the largest effect ($K_d = 0.58$ nM), which is comparable to the result observed in absence of the entire suppressor region from receptors N terminus (Δ(1-223) T604). Mutations L30K, L32K, D34K, R36E, R54E, and K127E also significantly increased IP_3 binding affinity. These residues are all clustered on the molecular surface of the IP_3R_{sup} Head subdomain (Figures 3C and 3D) and could potentially interact simultaneously with IP_3R_{core}.

While the aforementioned mutagenesis studies mapped a potential binding site of IP_3R_{core} on IP_3R_{sup}, the IP_3R_{sup} binding site on IP_3R_{core} is currently unknown. A manual inspection of the IP_3 bound IP_3R_{core} structure could not identify any potential IP_3R_{sup} binding site, which meets our criteria on the basis of surface complementarity, charge distribution, and sequence conservation. This may be due to the fact that it is the ligand-free form, not the IP_3 bound form that interacts with IP_3R_{sup}. Indeed, previous EM study (Sato et al., 2004) has suggested a change in the orientation of the two

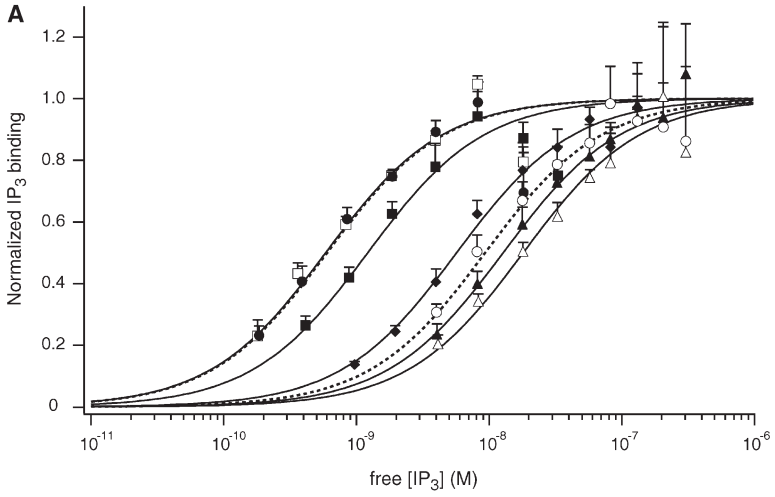

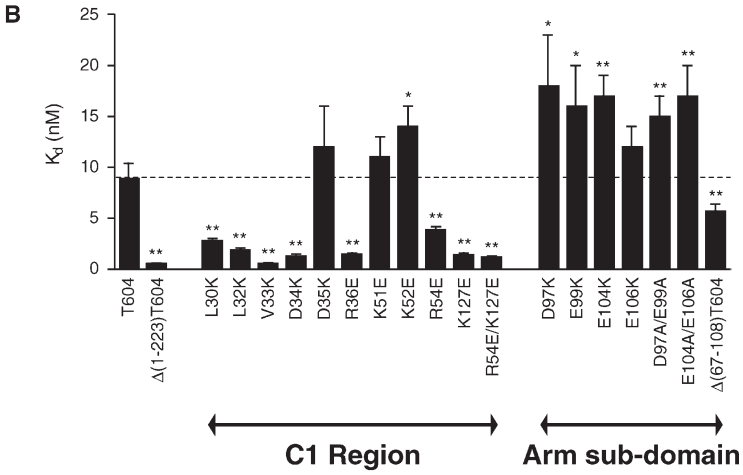

Figure 4. IP_3 Binding Affinity of Site-Directed Mutants T604

(A) IP_3 binding curves of wild-type T604 (open circles), Δ(1-223)T604 (closed circles), V33K (open squares), D34K (closed squares), E104K (open triangles), E106K (closed triangles), and Δ(67-108)T604 (closed diamonds). The values were normalized against the maximum IP_3 binding estimated in each experiment and were averaged (n = 3 or 4). Error bars correspond to the standard deviation and only upper sides are indicated. The data were fitted with Hill-Langmuir equation.

(B) The IP_3 dissociation constants for wild-type T604 and various mutants. The values are averaged of three or four measurements. Error bars correspond to standard deviation. *$p < 0.05$ and **$p < 0.01$ (Student's t test, compared with the value of T604).

domains within IP_3R_{core} upon IP_3 binding. Because of these uncertainties, the exact structural basis for this intramolecular interaction, which is critical for IP_3 binding, still remains unclear.

The IP_3-Supressor Domain as a Focal Point for Protein-Protein Interactions

Recent studies identified the first 223 residues of the IP_3R to be a binding target of numerous proteins including CaM (Adkins et al., 2000; Sienaert et al., 2002), CaBP1 (Kasri et al., 2004b; Yang et al., 2002), Homer (Tu et al., 1998), and RACK1 (Patterson et al., 2004). Biochemically characterized binding sites for these interacting partners have been mapped onto the current structure of IP_3R_{sup} (Figures 3C and 3D). The two polypeptide segments, termed P1 (residues P49–N81) and P2 (residues E106–S128), located at the joint between the Head and Arm subdomains, have been implicated in CaM binding (Sienaert et al., 2002). Kasri and colleagues (Kasri et al., 2004b) recently reported that CaBP1 also binds to the P1 region, whereas others (Yang et al., 2002) indicated that part of IP_3R_{core} may also be involved in CaBP1 binding. The Homer binding site comprising residues ^{49}PPKKF^{53} is part of the conserved region of the IP_3R_{sup} (Tu et al., 1998). This motif is part of a loop region between the β3 and β4 strands, which is largely exposed to the solvent and, thus, accessible to the Homer protein.

In contrast to many binding partners targeting the Head subdomain of IP_3R_{sup}, the WD40 containing scaffold protein, RACK1, has its essential binding sites on the Arm subdomain (residues 90–110) and on the α domain within the IP_3R_{core} (residues 580–600) (Patterson et al., 2004). The first segment encompasses nearly all of the α3 helix in the Arm subdomain. Interestingly, RACK1 binding increased the affinity of IP_3R for IP_3 2-fold, therefore enhancing the sensitivity of the receptor to the IP_3 concentration within the cell. Furthermore, deletion of residues 90–110 from the entire receptor led to a 100-fold decrease in sensitivity to IP_3-induced Ca^{2+} release (Patterson et al., 2004). These results suggest that the Arm subdomain may play a role in channel regulation other than IP_3 affinity modulation. Taken together, many binding sites for the aforementioned cellular binding partners are located within the IP_3R_{sup}, underscoring the significance of IP_3R_{sup} as a focal point of the protein-

protein interactions that regulate channel activity of the receptor.

Ryanodine Receptor May Contain Similar β-Trefoil Domains

An earlier amino acid sequence analysis on IP_3R and its closely related Ca^{2+} ion channel RyR indicated that both receptors may share similar structural motifs at the N-terminal region (Furuichi et al., 1989; Henzi and MacDermott, 1992). In light of our IP_3R_{sup} structure, as well as our previous study on IP_3R_{core}, we revisited the significance of the sequence similarity in this region between IP_3R and RyR. Using mGenTHREADER (Jones, 1999), and some manual manipulation of sequence alignment between the two receptors, we derived structure-based sequence alignments between mIP_3R1 and human RyR type 1 (hRyR1), which clearly identified two β-trefoil domains within hRyR1 (Figure 5). The first domain spans residues 1–210 (E value of 6×10^{-6}), whereas the second encompasses residues 210–393 (E value of 3×10^{-4}) in hRyR1 (Figure 5). The β-trefoil fold is made up of three structural repeats giving rise to a pseudo 3-fold symmetry (Murzin et al., 1992). In the first β-trefoil domain of hRyR1, these repeats encompass residues 1–70, 71–151, and 152–203, respectively. The position of the second and third structural repeats corresponds to MIR1 (112-166) and MIR2 (173-223) structural elements in Ponting's earlier analysis (Ponting, 2000). In the second β-trefoil domain, the three structural repeats comprise residues 218–264, 265–318, and 319–392, respectively. Notably, MIR3 (231-287) corresponds to the position of the first structural repeats in the second domain, whereas MIR4 (270-360) spans the second and third repeats (Ponting, 2000).

Although the sequence conservation among members of this β-trefoil protein family is relatively low, many key hydrophobic residues essential for maintaining the β-trefoil structural architecture are invariant among the family members (Murzin et al., 1992). Indeed, IP_3Rs and RyRs possess the highest homology for those residues located at the bottom layer followed by the middle and top layer of the β-trefoil core structure (Figure 5A) (Murzin et al., 1992). In addition, significant conservation can be observed for some residues that make up the triangular cap. These structural features between the two receptors meet the proposed criteria for the β-trefoil protein family by Murzin et al. (Murzin et al., 1992). In contrast, a study by Baker and colleagues proposed that the region consisting of residues 41–420 of RyR1 has an oxidoreductase-like domain architecture (Baker et al., 2002). The present structural analysis of IP_3R and our structure-based sequence analysis between IP_3Rs and RyRs supports the proposal by Ponting (Ponting, 2000) and further suggests that the N-terminal portion of RyRs is comprised of two β-trefoil domains in a similar manner as IP_3Rs.

It is known that a number of mutations which lead to malignant hyperthermia (MH) and central core disease (CCD) are located within this segment of RyR1 (Figure 5) (Loke and MacLennan, 1998). Among all known MH and CCD mutations, some of the mutations (C35R [Lynch et al., 1997], R44C [Tammaro et al., 2003], and D166N [Rueffert et al., 2002]) can be mapped within β strands of the first and second β-trefoil domains. These mutations could cause significant instability in the β-trefoil architecture, as the corresponding residues in IP_3R all participate in hydrophobic core formation. On the contrary, other MH and CCD mutations (R163C [Quane et al., 1993], G215E [Romero et al., 2003], G248R [Gillard et al., 1992], R328W [Loke et al., 2003], and G341R [Quane et al., 1994]) are predicted to reside on loops linking the β strands. These mutations may change the surface properties of the receptor and therefore may lead to disruption of some key protein-protein interactions essential for the Ca^{2+}-gating function of the receptor.

Using the structures of the IP_3R β-trefoil domains and the structure-based sequence alignment between IP_3Rs and RyRs (Figure 5A), models of the two β-trefoil domains of hRyR1 (RyR-βD1 and RyR-βD2, respectively) were generated using Modeller (Sali and Blundell, 1993). Thirty models were calculated for RyR-βD1 and RyR-βD2 independently and a representative model for each domain is shown in Figures 5B–5E. These models support the existence of the two β-trefoil folds in RyR and even predict the presence of the Arm subdomain in RyR-βD1. In addition, three long loops are identified in RyR-βD2 between β4/β5, β8/β9, and β11/β12. Surface characteristic analysis (Figures 5B–5E, middle and lower panels) shows that RyR-βD1 is slightly more negatively charged than RyR-βD2 and that RyR-βD1 possesses a highly conserved region similar to the C1 region in IP_3R_{sup}. More importantly, our modeling analysis provides useful clues for understanding the molecular basis for MH- and CCD-associated mutations in humans. We found that three out of four mutations (C35R, R163C, and D166N) in RyR-βD1 reside on one side of the β-trefoil structure, whereas two out of four mutations found in RyR-βD2 (R328W, G341R) are localized to the long loop connecting β8 and β9 strands (Figures 5B–5E, top panels). It is intriguing to find two pathologically critical mutations in the long loop region of RyR-βD2. While the molecular function of the N-terminal portion of RyRs remains unclear, the presented structural analysis sheds light onto the structure-function elucidation of the receptor and its relationship to the closely related IP_3R.

Conclusions

Our present and previous study (Bosanac et al., 2002) revealed that the N-terminal region of IP_3R consists of two β-trefoil folds (residues 1–223 and 224–434) followed by the "armadillo"-like domain (438–604). The first β-trefoil domain is unique in that it contains a helix-turn-helix motif between the β4 and β5 strand, which extrudes away from the β-trefoil structure. These three domains interact with one another, and the two domain linkers, one connecting the first and second β-trefoil folds and the other joining the second β-trefoil fold and the "armadillo"-like domain, dictate the orientation of these three domains with respect to one another. Our mutagenesis analyses provide evidence for the interaction between the first β-trefoil domain and the latter two domains, which together constitute the IP_3 binding site. This intramolecular interaction probably controls the ability of the receptor to bind IP_3, hence influencing the affinity of the receptor for the ligand. The IP_3R_{core} binding

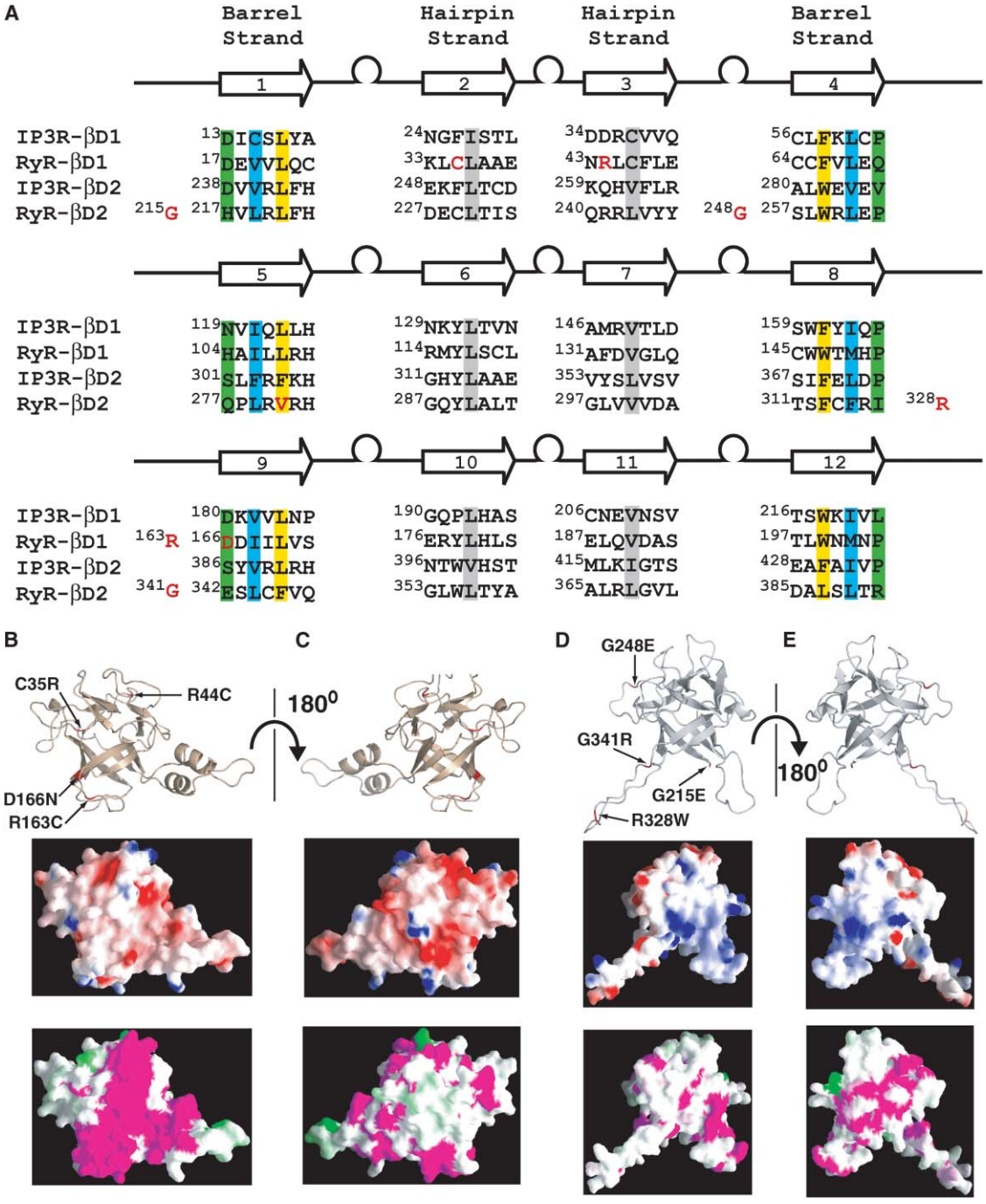

Figure 5. Modeling of β-Trefoil Domains in hRyR1

(A) Structure-based sequence alignment between mIP$_3$R1 and hRyR1. Location of the 12 β strands in the two β-trefoil domains of hRyR1 is depicted. Residues within the β strands of the two β-trefoil domains in mIP$_3$R1 (IP3R-βD1 and IP3R-βD2) and hRyR1 (RyR-βD1 and RyR-βD2) are shown. Residues comprising the linker regions are not shown. Key residues at the interior of the β-trefoil barrel are arranged in three layers referred to as bottom (highlighted in yellow), middle (highlighted in blue), and top (highlighted in green) (Murzin et al., 1992). The bottom layer is comprised of residues just underneath the triangular cap, with the middle and top layers lying parallel to it and away from the cap. The key residues of the triangular cap (highlighted in gray) interact with the residues from the bottom layer of the barrel. Residues of hRyR1 whose mutations lead to MH and CCD are shown in red.

(B) Modeled structure of first β-trefoil domain in hRyR1 (RyR-βD1) based on the sequence alignment shown in (A). The model is shown as ribbon diagram in a top panel, with MH and CCD mutations highlighted in red. Surface electrostatic potential, with positive charge depicted in blue and negative charge in red, is plotted in the middle panel. The bottom panel shows surface residue conservation determined from sequence alignment of RyR receptors listed below, with identical residues in magenta and the least conserved residues in green. The highly conserved area (residues R75, Q79, Q93, T99, Y102, R124, D128, K129, L130, F132, T148, H150, P151, A152, S153, K154, Q155, S157, E158, E160, K161, R163, I169, V171, S172, V173, E176, R177, Y178, F194) is observed only on this side of the molecule.

(C) View in (B) rotated by 180° with same panel arrangement as in (A).

site coincides with a large area of conserved molecular surface found on IP_3R_{sup}. Interestingly, some of the residues within this conserved surface have been previously shown to interact with CaM, CaBP1, and Homer. It is conceivable that this area of IP_3R_{sup} may be involved in the interplay between the IP_3R_{core} and other cellular binding partners for the purpose of regulating channel-gating function of the receptor. Finally, our bioinformatic analysis of hRyR1 suggests the presence of two β-trefoil domains in the N-terminal region of the RyRs, providing compelling clues toward understanding the molecular basis of MH and CCD mutations.

Experimental Procedures

Overexpression and Purification of IP_3R_{sup}

The mouse type 1 IP_3R protein fragment encompassing the suppressor domain (IP_3R_{sup}), residues 2–223, was cloned into pET-23a expression vector. The desired protein fragment was expressed with N-terminal T7 tag and C-terminal poly-His tag. Expression was carried out in BL21-CodonPlus(DE3)-RIL *E. coli* strain (Stratagene) at 15°C for approximately 15 hr using 0.5 mM IPTG induction. T7-IP_3R_{sup}-6His was first purified with Ni-NTA resin (Qiagen) followed by size exclusion chromatography (Superdex 75, Amersham-Pharmacia). The two tags were not removed during the purification due to absence of a protease cleavage site between the tags and the target protein. Seleno-methionine (Se-Met)-labeled protein was produced in minimal media which inhibits methionine biosynthesis (Van Duyne et al., 1993). Incorporation of Se-Met was confirmed by electrospray mass spectrometry. The purified protein was concentrated to 10 mg/ml in a crystallization buffer (15 mM Tris-HCl [pH 8.0], 300 mM NaCl, 5% v/v glycerol, and 2 mM Tris (2-carboxyethyl)phosphine [TCEP]).

Crystallization and Data Collection

Crystals of T7-IP_3R_{sup}-6His were grown by a hanging-drop vapor diffusion method at 22°C by combining 2 μl of protein solution with 2 μl of reservoir solution (100 mM Tris-HCl [pH 7.8], 4%–6% PEG 6000, 2.0 M NaCl, and 2 mM TCEP). Crystals grew as single rods (dimensions 0.30 × 0.15 × 0.15 mm) within 7 days. They were flash cooled in reservoir buffer supplemented with 20% v/v glycerol. MAD and native data were collected at 100 K on a 19-BM beam line at the APS Synchrotron facility and were processed with HKL2000 (Otwinowski and Minor, 1997). Crystals belonged to the hexagonal R32 space group with cell dimensions a = 147.3 Å, b = 147.3 Å, and c = 65.0 Å, and with one molecule in the asymmetric unit.

Structure Determination and Refinement

Positions of two selenium atoms (Se-Met63 and Se-Met147) were determined by Solve (Terwilliger et al., 1987) at resolution of 2.0 Å with a figure of merit 0.74. Density modification and solvent flattening with the program CNS (Brunger et al., 1998) increased the overall figure of merit to 0.97. The experimental electron density map was of exceptional quality (Figure 2C) with no density observed for T7 and poly-His tags. Model building was carried out in the program O (Jones et al., 1991) and refinement with CNS (Brunger et al., 1998). The final model comprised residues 7–75 and 82–223 with 96.7% of residues in the most favored regions of the Ramachandran plot with 0.5% residues in the disallowed region. In total, 1841 atoms with a mean temperature factor at 36.2 $Å^2$ were observed: 1705 protein atoms (⟨B⟩ of 36.0 $Å^2$) and 132 solvent atoms (⟨B⟩ of 38.2 $Å^2$). The R_{cryst} and R_{free} of the final model were 20.5 and 23.8, respectively.

Design and Preparation of Proteins for IP_3 Binding Assays

Site-directed mutagenesis of T604 was performed with pET-T604 (Yoshikawa et al., 1999a) and primers containing appropriate substitutions (Supplemental Table S2), according to the method described previously (Sawano and Miyawaki, 2000). A mutant T604 in which amino acid residues 67–108 were deleted was constructed as follows. The PCR product from pET-T604 using primers P-17 and P-19 (Supplemental Table S2) was digested with XbaI and EcoRI, and the PCR product from pET-T604 using primers P-18 and P-20 (Supplemental Table S2) was digested with EcoRI and BamHI. These fragments were inserted into the XbaI and BamHI sites of pET-3a (Novagen) to generate pET-Δ(67-108)-T604. All mutations were confirmed by DNA sequencing.

Expression of recombinant proteins in *E. coli* BL21-CodonPlus(DE3)-RIL (Stratagene) was carried out as described previously (Yoshikawa et al., 1999a) with minor modifications. To avoid tracer depletion in the IP_3 binding assay, the expression amounts of the recombinant proteins were optimized for each mutant by changing the incubation time from 1.5 to 20 hr after IPTG induction. Cells obtained from 2 ml culture were resuspended in 0.4 ml cytosol-like medium (CLM: 110 mM KCl, 10 mM NaCl, 5 mM KH_2PO_4, and 50 mM HEPES-KOH [pH 7.4], at 4°C) containing 1 mM DTT, 0.5 mM EGTA, and protease inhibitors (10 μM E-64, 10 μM leupeptin, 10 μM pepstatin A, and 100 μM phenylmethylsulfonyl fluoride). After disruption of the cells by sonication, the total cell lysate was centrifuged. The supernatant (soluble proteins) was frozen in liquid nitrogen, and stored at −80°C until use. Protein concentration was determined with the protein assay kit (Bio-Rad) using BSA as a standard.

IP_3 Binding Assay

Soluble proteins (0.5 μg) were diluted to 100 μl with CLM containing 1 mM DTT and 0.5 mM EGTA, and incubated for 10 min on ice with 0.068–8.7 nM (^{3}H)IP_3 (PerkinElmer Life Sciences) and various concentration (10–300 nM) of unlabeled IP_3 (Dojindo). After the addition of 4 μl of 50 mg/ml γ-globulin and 100 μl of 30% (w/v) polyethylene glycol 6000 in CLM, the mixture was incubated for 5 min on ice and centrifuged at 20,000 × g for 5 min at 4°C. The resultant pellet was dissolved in 180 μl of Solvable (Packard), neutralized with 18 μl of acetic acid, and its radioactivity was measured in 5 ml of Atomlight (Packard) with a liquid scintillation counter LS-6500 (Beckman). Nonspecific IP_3 binding was determined by the linear relationship between total IP_3 concentration and the amount of IP_3 binding to nonreceptor sites, using soluble protein prepared from *E. coli* cells transformed with pET-23a vector (Novagen). Nonlinear regression of IP_3 binding data was performed with Igor Pro 4.08 Carbon software (WaveMetrics).

Acknowledgments

We thank the staff of X19-BM at APS for help in data collection, Gil Privé for discussions on data analysis, David Jones for mGenTHREADER analysis, and Dina Schneidman for help with molecular modeling. We are grateful to Ikuko Hayashi, Michael Plevin, Jane Gooding, Brigitte Maurer, Jenny Chan, and Tapas Kumar Mal for assistance on many aspects of this work, and David MacLennan and Natasha Kraeva for providing us with the latest information on MH and CCD mutations. We are also thankful to lab members of Mitsu Ikura, Emil Pai, David Rose, and Gil Privé for helpful discus-

(D) Model of second β-trefoil domain structure of hRyR1 (RyR-βD2) in the same orientation as RyR-βD1 shown in (B).
(E) View in (D) rotate by 180°. Panel arrangement is the same as that in (B). For more detail on the modeled structures of RyR-βD1 and RyR-βD2 see Supplemental Figure S1. National Center for Biotechnology Information (NCBI) accession numbers for sequences used in the sequence alignment of RyRs are human RyR1 (J05200), human RyR2 (X98330), human RyR3 (AJ001515), rabbit RyR1 (X15209), rabbit RyR2 (M59743), rabbit RyR3 (X68650), bull frog RyR1 (D21070), bull frog RyR3 (D21071), fruit fly RyR (D17389), and *C. elegans* RyR (D45899). Homology modeling was performed using Modeller (Sali and Blundell, 1993). Conservation was determined with ConSurf (Armon et al., 2001) and surface representation was generated with GRASP (Nicholls et al., 1991) (middle and bottom panels of [B]–[E]). PyMol (DeLano, 2002) was used in top panels of (B)–(E).

sions. This work was supported by a fellowship from the Canadian Institute of Health and Research to I.B., by a grant from the Heart and Stroke Foundation of Canada to M.I., and by grants from the Ministry of Education, Science, Sports, and Culture of Japan to M.K. M.I. was a recipient of a CIHR Senior Investigator Award and is now a Canada Research Chair in Cancer Structural Biology.

Received: October 9, 2004
Revised: November 15, 2004
Accepted: November 24, 2004
Published: January 20, 2005

References

Adkins, C.E., Morris, S.A., De Smedt, H., Sienaert, I., Torok, K., and Taylor, C.W. (2000). Ca2+-calmodulin inhibits Ca2+ release mediated by type-1, -2 and -3 inositol trisphosphate receptors. Biochem. J. *345*, 357–363.

Armon, A., Graur, D., and Ben-Tal, N. (2001). ConSurf: an algorithmic tool for the identification of functional regions in proteins by surface mapping of phylogenetic information. J. Mol. Biol. *307*, 447–463.

Baker, M.L., Serysheva, I.I., Sencer, S., Wu, Y., Ludtke, S.J., Jiang, W., Hamilton, S.L., and Chiu, W. (2002). The skeletal muscle Ca2+ release channel has an oxidoreductase-like domain. Proc. Natl. Acad. Sci. USA *99*, 12155–12160.

Berridge, M.J. (1993). Inositol trisphosphate and calcium signalling. Nature *361*, 315–325.

Berridge, M.J., Bootman, M.D., and Roderick, H.L. (2003). Calcium signaling: dynamics, homeostasis and remodeling. Nat. Rev. Mol. Cell Biol. *4*, 517–529.

Bosanac, I., Alattia, J.R., Mal, T.K., Chan, J., Talarico, S., Tong, F.K., Tong, K.I., Yoshikawa, F., Furuichi, T., Iwai, M., et al. (2002). Structure of the inositol 1,4,5-trisphosphate receptor binding core in complex with its ligand. Nature *420*, 696–700.

Brunger, A.T., Adams, P.D., Clore, G.M., DeLano, W.L., Gros, P., Grosse-Kunstleve, R.W., Jiang, J.S., Kuszewski, J., Nilges, M., Pannu, N.S., et al. (1998). Crystallography & NMR system: a new software suite for macromolecular structure determination. Acta Crystallogr. D Biol. Crystallogr. *54*, 905–921.

da Fonseca, P.C., Morris, S.A., Nerou, E.P., Taylor, C.W., and Morris, E.P. (2003). Domain organization of the type 1 inositol 1,4,5-trisphosphate receptor as revealed by single-particle analysis. Proc. Natl. Acad. Sci. USA *100*, 3936–3941.

DeLano, W.L. (2002). The PyMOL Molecular Graphics System (San Carlos, CA: DeLano Scientific).

Furuichi, T., and Mikoshiba, K. (1995). Inositol *1*, 4, 5-trisphosphate receptor-mediated Ca2+ signaling in the brain. J. Neurochem. *64*, 953–960.

Furuichi, T., Yoshikawa, S., Miyawaki, A., Wada, K., Maeda, N., and Mikoshiba, K. (1989). Primary structure and functional expression of the inositol 1,4,5-trisphosphate-binding protein P400. Nature *342*, 32–38.

Furuichi, T., Kohda, K., Miyawaki, A., and Mikoshiba, K. (1994). Intracellular channels. Curr. Opin. Neurobiol. *4*, 294–303.

Gillard, E.F., Otsu, K., Fujii, J., Duff, C., de Leon, S., Khanna, V.K., Britt, B.A., Worton, R.G., and MacLennan, D.H. (1992). Polymorphisms and deduced amino acid substitutions in the coding sequence of the ryanodine receptor (RYR1) gene in individuals with malignant hyperthermia. Genomics *13*, 1247–1254.

Hamada, K., Terauchi, A., and Mikoshiba, K. (2003). Three-dimensional rearrangements within inositol 1,4,5-trisphosphate receptor by calcium. J. Biol. Chem. *278*, 52881–52889.

Henzi, V., and MacDermott, A.B. (1992). Characteristics and function of Ca2+- and inositol 1,4,5-trisphosphate-releasable stores of Ca2+ in neurons. Neuroscience *46*, 251–273.

Holm, L., and Sander, C. (1993). Protein structure comparison by alignment of distance matrices. J. Mol. Biol. *233*, 123–138.

Jiang, Q.X., Thrower, E.C., Chester, D.W., Ehrlich, B.E., and Sigworth, F.J. (2002). Three-dimensional structure of the type 1 inositol 1,4,5-trisphosphate receptor at 24 Å resolution. EMBO J. *21*, 3575–3581.

Jones, D.T. (1999). GenTHREADER: an efficient and reliable protein fold recognition method for genomic sequences. J. Mol. Biol. *287*, 797–815.

Jones, T.A., Zou, J.Y., Cowan, S.W., and Kjeldgaard (1991). Improved methods for binding protein models in electron density maps and the location of errors in these models. Acta Crystallogr. A *47*, 110–119.

Kasri, N.N., Bultynck, G., Smyth, J., Szlufcik, K., Parys, J.B., Callewaert, G., Missiaen, L., Fissore, R.A., Mikoshiba, K., and de Smedt, H. (2004a). The N-terminal Ca2+-independent calmodulin-binding site on the inositol 1,4,5-trisphosphate receptor is responsible for calmodulin inhibition, even though this inhibition requires Ca2+. Mol. Pharmacol. *66*, 276–284.

Kasri, N.N., Holmes, A.M., Bultynck, G., Parys, J.B., Bootman, M.D., Rietdorf, K., Missiaen, L., McDonald, F., Smedt, H.D., Conway, S.J., et al. (2004b). Regulation of InsP3 receptor activity by neuronal Ca2+-binding proteins. EMBO J. *23*, 312–321.

Kraulis, P.J. (1991). MOLSCRIPT: a program to produce both detailed and chematic plots of protein structure. J. Appl. Crystallogr. *24*, 946–950.

Kume, S., Muto, A., Inoue, T., Suga, K., Okano, H., and Mikoshiba, K. (1997). Role of inositol 1,4,5-trisphosphate receptor in ventral signaling in Xenopus embryos. Science *278*, 1940–1943.

Lawrence, M.C., and Bourke, P. (2000). CONSCRIPT: a program for generating electron density isosurfaces for presentation in protein crystallography. J. Appl. Crystallogr. *33*, 990–991.

Loke, J., and MacLennan, D.H. (1998). Malignant hyperthermia and central core disease: disorders of Ca2+ release channels. Am. J. Med. *104*, 470–486.

Loke, J.C., Kraev, N., Sharma, P., Du, G., Patel, L., Kraev, A., and MacLennan, D.H. (2003). Detection of a novel ryanodine receptor subtype 1 mutation (R328W) in a malignant hyperthermia family by sequencing of a leukocyte transcript. Anesthesiology *99*, 297–302.

Lynch, P.J., Krivosic-Horber, R., Reyford, H., Monnier, N., Quane, K., Adnet, P., Haudecoeur, G., Krivosic, I., McCarthy, T., and Lunardi, J. (1997). Identification of heterozygous and homozygous individuals with the novel RYR1 mutation Cys35Arg in a large kindred. Anesthesiology *86*, 620–626.

Matsumoto, M., Nakagawa, T., Inoue, T., Nagata, E., Tanaka, K., Takano, H., Minowa, O., Kuno, J., Sakakibara, S., Yamada, M., et al. (1996). Ataxia and epileptic seizures in mice lacking type 1 inositol 1,4,5- trisphosphate receptor. Nature *379*, 168–171.

Merrit, E.A., and Bacon, D.J. (1997). Raster3D: photorealistic molecular graphics. In Methods in Enzymology, Volume 277: Macromolecular Crystallography, Part B, C.W. Carter and R.M. Sweet, eds. (New York: Academic Press), pp. 505–524.

Murzin, A.G., Lesk, A.M., and Chothia, C. (1992). β-trefoil fold. Patterns of structure and sequence in the Kunitz inhibitors interleukins-1 β and 1 α and fibroblast growth factors. J. Mol. Biol. *223*, 531–543.

Nicholls, A., Sharp, K.A., and Honig, B. (1991). Protein folding and association: insights from the interfacial and thermodynamic properties of hydrocarbons. Proteins *11*, 281–296.

Otwinowski, Z., and Minor, W. (1997). Processing of X-ray diffraction data collected in oscillation mode. In Methods in Enzymology, Volume 276: Macromolecular Crystallography, Part A, C.W. Carter and R.M. Sweet, eds. (New York: Academic Press), pp. 307–326.

Patterson, R.L., van Rossum, D.B., Barrow, R.K., and Snyder, S.H. (2004). RACK1 binds to inositol 1,4,5-trisphosphate receptors and mediates Ca2+ release. Proc. Natl. Acad. Sci. USA *101*, 2328–2332.

Ponting, C.P. (2000). Novel repeats in ryanodine and IP3 receptors and protein O-mannosyltransferases. Trends Biochem. Sci. *25*, 48–50.

Quane, K.A., Healy, J.M., Keating, K.E., Manning, B.M., Couch, F.J., Palmucci, L.M., Doriguzzi, C., Fagerlund, T.H., Berg, K., Ording, H., et al. (1993). Mutations in the ryanodine receptor gene in central core disease and malignant hyperthermia. Nat. Genet. *5*, 51–55.

Quane, K.A., Keating, K.E., Manning, B.M., Healy, J.M., Monsieurs, K., Heffron, J.J., Lehane, M., Heytens, L., Krivosic-Horber, R., Adnet, P., et al. (1994). Detection of a novel common mutation in the ryanodine receptor gene in malignant hyperthermia: implications for diagnosis and heterogeneity studies. Hum. Mol. Genet. *3*, 471–476.

Romero, N.B., Monnier, N., Viollet, L., Cortey, A., Chevallay, M., Leroy, J.P., Lunardi, J., and Fardeau, M. (2003). Dominant and recessive central core disease associated with RYR1 mutations and fetal akinesia. Brain *126*, 2341–2349.

Rueffert, H., Olthoff, D., Deutrich, C., Meinecke, C.D., and Froster, U.G. (2002). Mutation screening in the ryanodine receptor 1 gene (RYR1) in patients susceptible to malignant hyperthermia who show definite IVCT results: identification of three novel mutations. Acta Anaesthesiol. Scand. *46*, 692–698.

Rutenber, E., and Robertus, J.D. (1991). Structure of ricin B-chain at 2.5 Å resolution. Proteins *10*, 260–269.

Sali, A., and Blundell, T.L. (1993). Comparative protein modelling by satisfaction of spatial restraints. J. Mol. Biol. *234*, 779–815.

Sato, C., Hamada, K., Ogura, T., Miyazawa, A., Iwasaki, K., Hiroaki, Y., Tani, K., Terauchi, A., Fujiyoshi, Y., and Mikoshiba, K. (2004). Inositol 1,4,5-trisphosphate receptor contains multiple cavities and L-shaped ligand-binding domains. J. Mol. Biol. *336*, 155–164.

Sawano, A., and Miyawaki, A. (2000). Directed evolution of green fluorescent protein by a new versatile PCR strategy for site-directed and semi-random mutagenesis. Nucleic Acids Res. *28*, E78.

Serysheva, I.I., Bare, D.J., Ludtke, S.J., Kettlun, C.S., Chiu, W., and Mignery, G.A. (2003). Structure of the type 1 inositol 1,4,5-trisphosphate receptor revealed by electron cryomicroscopy. J. Biol. Chem. *278*, 21319–21322.

Sienaert, I., Nadif Kasri, N., Vanlingen, S., Parys, J.B., Callewaert, G., Missiaen, L., and De Smedt, H. (2002). Localization and function of a calmodulin/apocalmodulin binding domain in the N-terminal part of the type 1 inositol 1,4,5-trisphosphate receptor. Biochem. J. *365*, 269–277.

Tammaro, A., Bracco, A., Cozzolino, S., Esposito, M., Di Martino, A., Savoia, G., Zeuli, L., Piluso, G., Aurino, S., and Nigro, V. (2003). Scanning for mutations of the ryanodine receptor (RYR1) gene by denaturing HPLC: detection of three novel malignant hyperthermia alleles. Clin. Chem. *49*, 761–768.

Taylor, C.W., Genazzani, A.A., and Morris, S.A. (1999). Expression of inositol trisphosphate receptors. Cell Calcium *26*, 237–251.

Terwillinger, T.C., Kim, S.H., and Eisenberg, J. (1987). Generalized method of determining heavy-atom positions using the difference Patterson function. Acta Crystallogr. A *43*, 1–5.

Transue, T.R., Smith, A.K., Mo, H., Goldstein, I.J., and Saper, M.A. (1997). Structure of benzyl T-antigen disaccharide bound to *Amaranthus caudatus* agglutinin. Nat. Struct. Biol. *4*, 779–783.

Tu, J.C., Xiao, B., Yuan, J.P., Lanahan, A.A., Leoffert, K., Li, M., Linden, D.J., and Worley, P.F. (1998). Homer binds a novel proline-rich motif and links group 1 metabotropic glutamate receptors with IP3 receptors. Neuron *21*, 717–726.

Van Duyne, G.D., Standaert, R.F., Karplus, P.A., Schreiber, S.L., and Clardy, J. (1993). Atomic structures of the human immunophilin FKBP-12 complexes with FK506 and rapamycin. J. Mol. Biol. *229*, 105–124.

Worley, P.F., Baraban, J.M., Colvin, J.S., and Snyder, S.H. (1987). Inositol trisphosphate receptor localization in brain: variable stoichiometry with protein kinase C. Nature *325*, 159–161.

Yang, J., McBride, S., Mak, D.O., Vardi, N., Palczewski, K., Haeseleer, F., and Foskett, J.K. (2002). Identification of a family of calcium sensors as protein ligands of inositol trisphosphate receptor Ca2+ release channels. Proc. Natl. Acad. Sci. USA *99*, 7711–7716.

Yoshikawa, F., Morita, M., Monkawa, T., Michikawa, T., Furuichi, T., and Mikoshiba, K. (1996). Mutational analysis of the ligand binding site of the inositol 1,4,5- trisphosphate receptor. J. Biol. Chem. *271*, 18277–18284.

Yoshikawa, F., Iwasaki, H., Michikawa, T., Furuichi, T., and Mikoshiba, K. (1999a). Trypsinized cerebellar inositol 1,4,5-trisphosphate receptor. Structural and functional coupling of cleaved ligand binding and channel domains. J. Biol. Chem. *274*, 316–327.

Yoshikawa, F., Uchiyama, T., Iwasaki, H., Tomomori-Satoh, C., Tanaka, T., Furuichi, T., and Mikoshiba, K. (1999b). High efficient expression of the functional ligand binding site of the inositol 1,4,5-triphosphate receptor in *Escherichia coli*. Biochem. Biophys. Res. Commun. *257*, 792–797.

Accession Numbers

The atomic coordinates for mIP_3R1_{sup} have been deposited in the Protein Data Bank with the accession number 1XZZ.